Available online at www.sciencedirect.com
ScienceDirect
Journal of Sound and Vibration 304 (2007) 466–478
JOURNAL OF SOUND AND VIBRATION
www.elsevier.com/locate/jsvi

Instabilities due to instrumentation phase-lead and phase-lag in the feedback control of a simple vibrating system

M.J. Brennan*, K.A. Ananthaganeshan, S.J. Elliott

Institute of Sound & Vibration Research, Southampton University, Highfield, Southampton, SO17 1BJ, UK

Received 8 September 2005; received in revised form 20 December 2006; accepted 23 January 2007

Abstract

In many active vibration control systems, it is the high frequency dynamic behaviour of the system that limits controller gain. However, in the specific case of vibration isolation, the low frequency dynamics of the system have an important role in the performance of the system. The main problem is the phase advance due to the high-pass filters that are necessary in such a system to remove the DC signal in the feedback loop. To investigate this problem the active control of a simple vibrating system is considered in this paper. Displacement, velocity and acceleration feedback control are studied, and the effects of the high-pass filters on the system stability are investigated. A simple system is specifically chosen to facilitate physical insight. For comparison, the limit on stability due to the high frequency dynamics, is also quantified by assuming a fixed time delay in the feedback loop. Simple expressions that give the maximum control gain in each case are derived. These expressions give insight into how the physical parameters govern the limits on stability. It is shown that for velocity feedback control it is desirable to have a high natural frequency of the mechanical system compared to the corner frequency of the high-pass filter. For displacement control, when there is phase-lag in the system, it is desirable to have high damping, and this is also the case for acceleration feedback when there is phase-lead. Some experimental work is presented to support the theoretical results.

1. Introduction

Direct velocity feedback has been recognised as a simple and robust control strategy for a number of years [1,2]. It has recently been applied to the problem of vibration isolation of delicate equipment from a host structure [3–5]. Acceleration and displacement feedback have also been proposed as ways of changing the dynamic characteristics of a structure [6–8]. Recent work on active vibration isolation of equipment using decentralised velocity feedback control has shown that the gain in the feedback loops has been limited by instabilities at low frequencies due to the instrumentation [3,4]. In other systems, the feedback gain may be limited by a high frequency instability which can be caused by phase-lag in the feedback loop due to the limited bandwidth of actuators [9], which is sometimes analysed by assuming a fixed time delay in the control loop [10]. Goh and Caughey [11] showed that although a velocity feedback control strategy using collocated

*Corresponding author. Tel.: +44 23 8059 2936; fax: +44 23 8059 3190.
E-mail address: mjb@isvr.soton.ac.uk (M.J. Brennan).

0022-460X/$ - see front matter © 2007 Elsevier Ltd. All rights reserved.
doi:10.1016/j.jsv.2007.01.046

actuators and sensors is unconditionally stable in principle, the dynamics of the actuators can destabilise the system. They proposed an alternative position feedback control strategy that improved the situation, and for which the stability conditions could be derived analytically. Fanson and Caughey [12] followed this with some experimental work to validate the strategy, and Friswell and Inman [13] subsequently compared these two control strategies. These papers tackle the problem of maintaining stability in large space structures. This approach of tackling the control of complex structures, where the high frequency dynamics of the system can cause instabilities, is a common theme in the control literature. In the specific case of active vibration isolation, however, the high frequency dynamics are arguably of less importance, because of the low-pass filtering properties of the system; it is the low frequency dynamics of the control system that are of greater importance when velocity and displacement are fed back. To gain insight into how the physical parameters govern the instabilities caused by instrumentation, active control of a single-degree-of-freedom (sdof) system is studied in this paper. For completeness, displacement, velocity and acceleration feedback are considered. For comparison, the factors that govern the instabilities that occur due to high frequency dynamics are presented using a similar approach to that in Ref. [10].

It is not the intention of the paper to propose new control strategies or to investigate the effectiveness of frequency dependent or model-based controllers, but rather to highlight the limitations of the simple control strategies outlined above. Because the analysis is performed on a sdof system, simple formulae can be derived which give the maximum gain that can be applied for each control system and the frequency at which the system becomes unstable. The results of the analysis allow some simple design guidelines to be formulated for active vibration isolation systems. These were subsequently applied in the design of a demonstrator for active vibration isolation, and this is reported in Ref. [14]. To support the theoretical predictions some experimental work is presented.

2. Closed-loop response of an idealised system

An elementary study of the active vibration isolation of a rigid-body can be conducted by analysing a base-excited sdof system with a control force applied in parallel with the spring and damper. To simplify the analysis even further, the system mass is assumed to be excited by a primary force, because the results of the analysis are directly applicable to the base-excited system.

Consider a sdof mass-spring-damper system with feedback control as shown in Fig. 1a. A massless passive mount with stiffness k and damping coefficient c supports a rigid mass m, which is excited by a primary force f_p. A control shaker generating the control force f_s is also installed between the mass and base structure in parallel with the passive mount. Direct negative feedback control is used, where the gains are positive and the

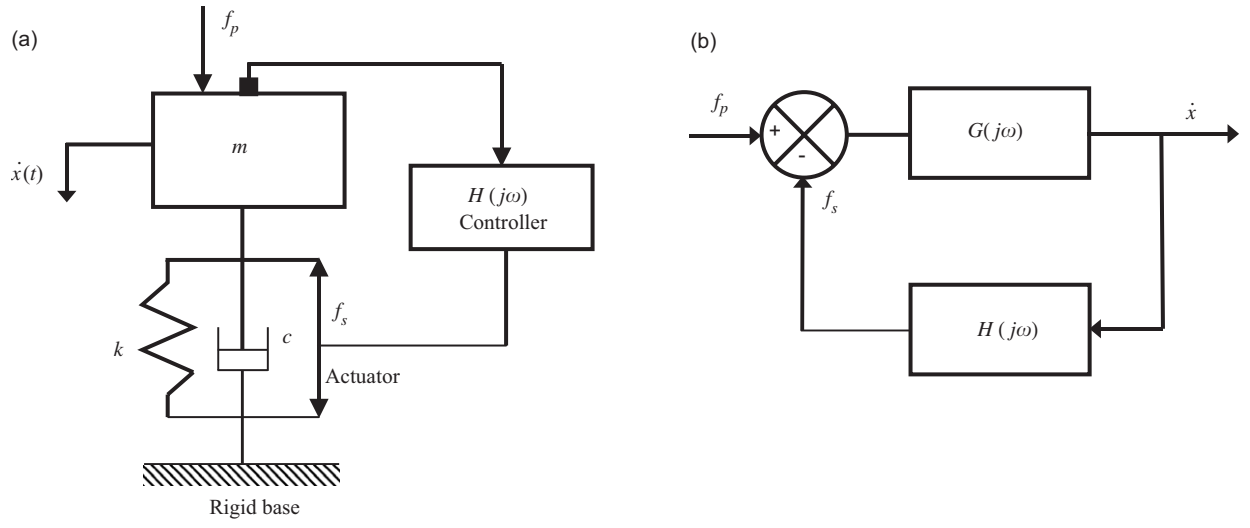

Fig. 1. Feedback control of a single-degree-of-freedom system: (a) physical representation and (b) block diagram representation.

control force is proportional to acceleration, velocity or displacement. A block diagram representation of the system is given in Fig. 1b, where the non-dimensional closed-loop frequency response (mobility) is given by

$$\frac{c\dot{X}(\mathrm{j}\Omega)}{F_p(\mathrm{j}\Omega)} = \frac{G(\mathrm{j}\Omega)}{1 + G(\mathrm{j}\Omega)H(\mathrm{j}\Omega)}, \tag{1}$$

where $f_p = F_p e^{\mathrm{j}\omega t}$, $x = Xe^{\mathrm{j}\omega t}$, and $G(\mathrm{j}\Omega)$ and $H(\mathrm{j}\Omega)$ are the plant and the controller frequency response functions respectively, and $\Omega = \omega/\omega_n$ is the forcing frequency normalised to the natural frequency of the system, $\omega_n = \sqrt{k/m}$. The uncontrolled response of the system, or plant response is given by

$$G(\mathrm{j}\Omega) = \frac{c\dot{X}(\mathrm{j}\Omega)}{F_p(\mathrm{j}\Omega)} = \frac{\mathrm{j}2\zeta\,\Omega}{1 - \Omega^2 + \mathrm{j}2\zeta\Omega}, \tag{2}$$

where $\zeta = c/(2\sqrt{mk})$ is the damping ratio of the system. For acceleration feedback control $H(\mathrm{j}\Omega) = \mathrm{j}\Omega(g/m)(1/2\zeta)$, for velocity feedback control $H(\mathrm{j}\Omega) = g/c$, and for displacement feedback control, $H(\mathrm{j}\Omega) = (1/\mathrm{j}\Omega)(g/k)(1/2\zeta)$, where g/m, g/c and g/k are the normalised feedback gains. Substituting for $G(\mathrm{j}\Omega)$ and the appropriate $H(\mathrm{j}\Omega)$ into Eq. (1), the non-dimensionalised closed-loop mobility can be derived for acceleration, velocity and displacement feedback control

Acceleration feedback:

$$\frac{c\dot{X}(\mathrm{j}\Omega)}{F_p(\mathrm{j}\Omega)} = \frac{\mathrm{j}2\zeta\,\Omega}{1 - \left(1 + \dfrac{g}{m}\right)\Omega^2 + \mathrm{j}2\zeta\Omega}. \tag{3a}$$

Velocity feedback:

$$\frac{c\dot{X}(\mathrm{j}\Omega)}{F_p(\mathrm{j}\Omega)} = \frac{\mathrm{j}2\zeta\,\Omega}{1 - \Omega^2 + \mathrm{j}2\zeta\,\Omega\left(1 + \dfrac{g}{c}\right)}. \tag{3b}$$

Displacement feedback:

$$\frac{c\dot{X}(\mathrm{j}\Omega)}{F_p(\mathrm{j}\Omega)} = \frac{\mathrm{j}2\zeta\,\Omega}{\left(1 + \dfrac{g}{k}\right) - \Omega^2 + \mathrm{j}2\zeta\,\Omega}. \tag{3c}$$

Fig. 2a shows the closed-loop non-dimensional mobility for acceleration, velocity and displacement feedback control respectively as a function of non-dimensional frequency for non-dimensional gains g/m, g/c

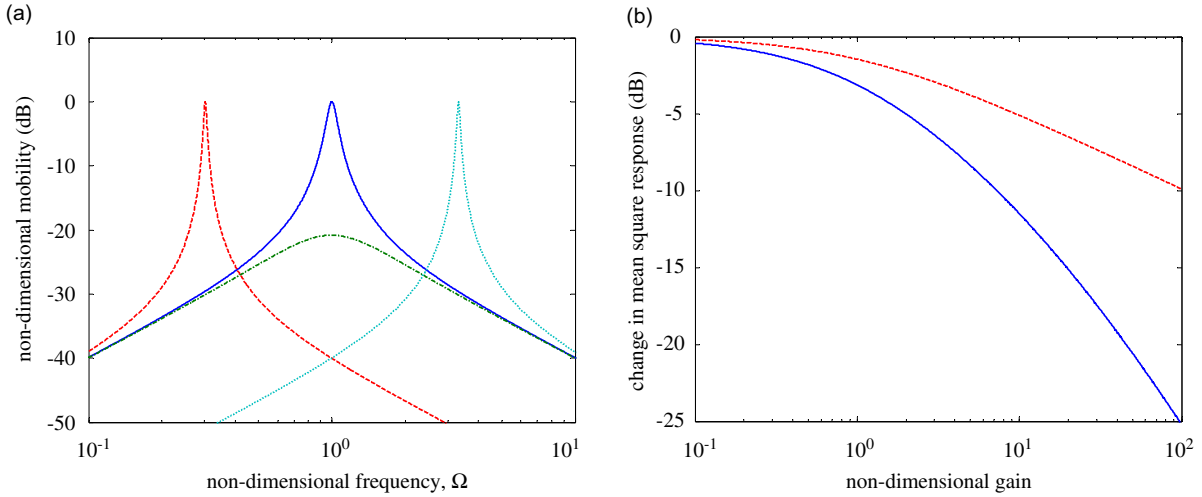

Fig. 2. Closed-loop response of a single-degree-of-freedom system, $\zeta = 0.05$. (a) Frequency response; no control, solid line; acceleration feedback, dashed line; velocity feedback, dashed dotted line; displacement feedback, dotted line. (b) Change in mean-square response in the frequency range $0.01 \leqslant \Omega \leqslant 100$; velocity feedback, solid line; acceleration and displacement feedback, dashed line.

and g/k of 10, and a damping ratio of 0.05. It can be seen that acceleration feedback reduces the response at the original resonance frequency and produces a resonance peak at a lower frequency. Acceleration feedback control effectively adds mass to the system. It can also be seen in Fig. 2a that velocity feedback effectively adds damping to the system, and that displacement feedback effectively adds stiffness to the system [7]. It is also noted that acceleration and displacement feedback tend to reduce the damping in the system, which manifests itself as narrower resonance peaks. The reason for this is evident from the expression for the damping ratio, because if either m or k is increased then the damping ratio is reduced.

If the system is excited by white noise then an appropriate measure to assess the effectiveness of the control strategies is the mean-square response of the system. This is normalised to the mean-square response of the system in the absence of control and is plotted for the three control strategies in Fig. 2b for the frequency range $.01 \leqslant \Omega \leqslant 100$. It can be seen that there is no difference between the reduction in the mean-square response of the system for displacement and acceleration feedback control, and that this is less than that for velocity feedback control.

The stability of the three systems can be determined by examining the Nyquist plots of their open-loop response functions, $G(\mathrm{j}\Omega)H(\mathrm{j}\Omega)$. The Nyquist criterion states that, assuming both the plant and controller are stable, the closed-loop system is stable if and only if $G(\mathrm{j}\Omega)H(\mathrm{j}\Omega)$ does not enclose the $(-1, 0)$ point in the complex plane [1]. For acceleration, velocity and displacement feedback control the open-loop response functions are respectively given by

Acceleration feedback:

$$G(\mathrm{j}\Omega)H(\mathrm{j}\Omega) = \left(\frac{g}{m}\right)\left(\frac{-\Omega^2}{1-\Omega^2+\mathrm{j}2\zeta\,\Omega}\right). \tag{4a}$$

Velocity feedback:

$$G(\mathrm{j}\Omega)H(\mathrm{j}\Omega) = \left(\frac{2\zeta g}{c}\right)\left(\frac{\mathrm{j}\Omega}{1-\Omega^2+\mathrm{j}2\zeta\Omega}\right). \tag{4b}$$

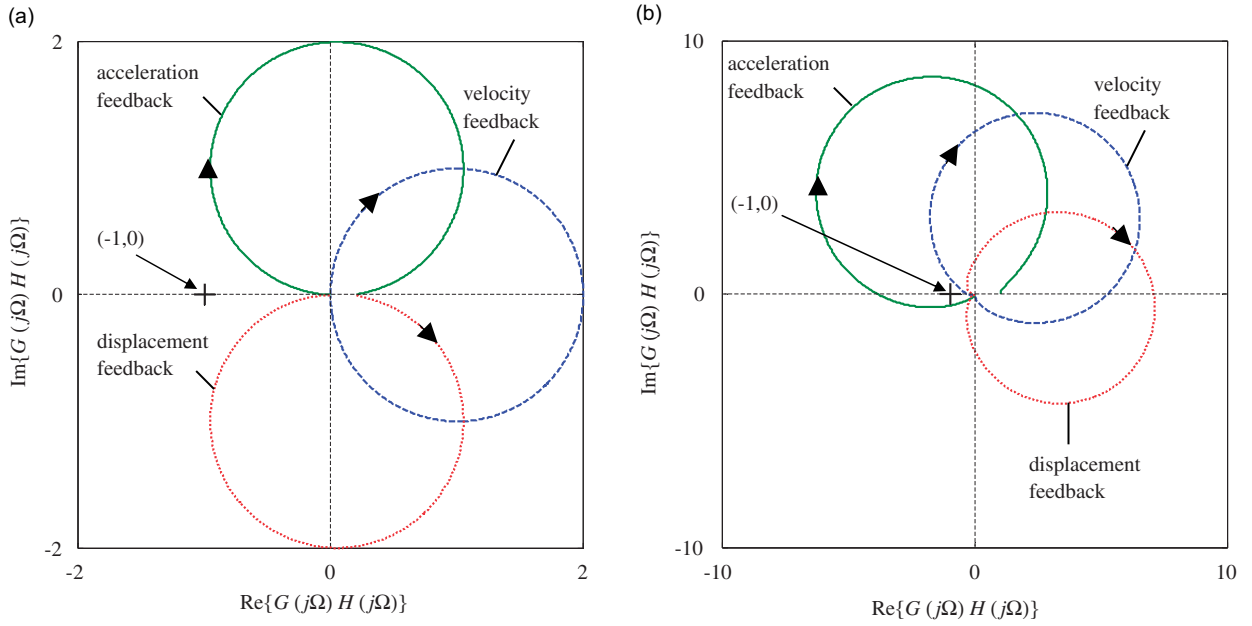

Fig. 3. Nyquist open-loop response plot of a single-degree-of-freedom system; acceleration feedback with one high-pass filter, solid line; velocity feedback with two high-pass filters, dashed line; displacement feedback with three high-pass filters, dotted line. (a) Ideal system, non-dimensional gain = 2. (b) Realistic system, $\alpha = 2$, non-dimensional gain = 10, acceleration feedback system has one high-pass filter, velocity feedback system has two high-pass filters and displacement feedback system has three high-pass filters.

Displacement feedback:

$$G(\mathrm{j}\Omega)H(\mathrm{j}\Omega) = \left(\frac{g}{k}\right)\left(\frac{1}{1-\Omega^2+\mathrm{j}2\zeta\Omega}\right). \tag{4c}$$

The Nyquist plots are shown in Fig. 3a. It can be seen that all of the control strategies are unconditionally stable.

3. Instability due to phase-lead

The limits on stability at low frequencies due to phase-lead discussed in this paper are because high-pass filters are included in the feedback loop. Accelerometers are often used in practice for measuring displacement and velocity as well as acceleration, and the electronic integration of the accelerometer output in practice can be represented by $(\alpha/\omega_n)(1/(1+\mathrm{j}\alpha\Omega))$, where $\alpha = \omega_n/\omega_c$ and ω_c is the -3 dB corner frequency. This can be interpreted as a high-pass filter $\mathrm{j}\omega_n\alpha\Omega/(\omega_n(1+\mathrm{j}\alpha\Omega))$ in series with an ideal integrator $1/(\mathrm{j}\omega_n\Omega)$. The term α/ω_n is included to ensure that the high-pass filter has a gain of unity at high frequencies. The device only operates as a pure integrator when $\alpha\Omega \gg 1$. Apart from each integrator, there are often additional high-pass filters in the feedback loop. One of these is normally in the conditioning amplifier for the accelerometer and the other can be found in the power amplifier. Thus for acceleration feedback control there may be up to two high-pass filters in the loop, for velocity feedback control there may be up to three, and for displacement feedback control there may be up to four.

The limits on stability are assessed by setting the imaginary part of the open-loop response function to zero, and solving the resulting equation to determine the frequency at which the system becomes unstable (critical frequency). This frequency is then substituted into the real part of the open-loop response function; if this is positive then the system is unconditionally stable and if it is negative then the real part is set to -1 and solved to give the maximum gain that can be applied before the system becomes unstable. For simplicity it is assumed that each high-pass filter has the same corner frequency.

Consider first the system with acceleration feedback control and a single high-pass filter. The open-loop frequency response function is given by

$$G(\mathrm{j}\Omega)H(\mathrm{j}\Omega) = \left(\frac{g}{m}\right)\left(\frac{-\Omega^2}{1-\Omega^2+\mathrm{j}2\zeta\,\Omega}\right)\left(\frac{\mathrm{j}\alpha\,\Omega}{1+\mathrm{j}\alpha\,\Omega}\right), \tag{5a}$$

which can be expanded into its real and imaginary parts to give

$$G(\mathrm{j}\Omega)H(\mathrm{j}\Omega) = \left(\frac{g}{m}\right)\left(\frac{-\alpha\Omega^4(2\zeta+\alpha(1-\Omega^2))}{((1-\Omega^2)^2+(2\zeta\Omega)^2)(1+\alpha^2\Omega^2)} + \mathrm{j}\frac{\alpha\Omega^3(2\alpha\zeta\Omega^2+\Omega^2-1)}{((1-\Omega^2)^2+(2\zeta\Omega)^2)(1+\alpha^2\Omega^2)}\right). \tag{5b}$$

Setting the imaginary part to zero and solving for the critical frequency gives $\Omega_c^2 = 1/(1+2\zeta\,\alpha)$. Substituting this into the real part of Eq. (5b), setting this equation to -1 and solving, gives an expression for the maximum gain

$$\frac{g_{\max}}{m} = 2\zeta\,\alpha\left(1+\frac{2\zeta}{\alpha}+\frac{1}{\alpha^2}\right). \tag{6a}$$

For low damping, i.e., $\zeta \ll 1$, and for a high-pass filter corner frequency much less than the natural frequency of the plant i.e., $\alpha \gg 1$, then Eq. (6a) reduces to

$$\frac{g_{\max}}{m} \approx 2\zeta\,\alpha. \tag{6b}$$

Note that the maximum gain is proportional to the mass, the ratio of the natural frequency of the system to the corner frequency of the high-pass filter, and the damping ratio.

Next, consider the velocity feedback control system with two high-pass filters. The open-loop frequency response function can be written as

$$G(\mathrm{j}\Omega)H(\mathrm{j}\Omega) = \left(\frac{g}{c}\right)\left(\frac{\mathrm{j}2\zeta\,\Omega}{1-\Omega^2+\mathrm{j}2\zeta\,\Omega}\right)\left(\frac{\mathrm{j}\alpha\,\Omega}{1+\mathrm{j}\alpha\,\Omega}\right)^2. \tag{7}$$

Following the procedure above results in a critical frequency of $\Omega_c \approx 1/\alpha$, and again assuming $\zeta \ll 1$ and $\alpha \gg 1$ gives a maximum gain of

$$\frac{g_{\max}}{c_{\mathrm{crit}}} \approx \alpha, \tag{8}$$

where $c_{\mathrm{crit}} = 2\sqrt{km}$ is the critical damping of the system.

Finally, consider the displacement feedback control system with three high-pass filters. The open-loop frequency response function can be written as

$$G(\mathrm{j}\Omega)H(\mathrm{j}\Omega) = \left(\frac{g}{k}\right)\left(\frac{1}{1-\Omega^2+\mathrm{j}2\zeta\,\Omega}\right)\left(\frac{\mathrm{j}\alpha\,\Omega}{1+\mathrm{j}\alpha\,\Omega}\right)^3. \tag{9}$$

Following a similar procedure and making the same assumptions as above gives a critical frequency of $\Omega_c = 1/\sqrt{3}\alpha$ and a maximum gain of

$$\frac{g_{\max}}{k} \approx 8. \tag{10}$$

The Nyquist plots for acceleration, velocity and displacement feedback control with one, two and three high pass filters respectively are shown in Fig. 3b, for $\alpha = 2$ (for clarity) $\zeta = 0.05$ and a non-dimensional gain of 10. It can be seen that all the plots cross the negative real axis and so are only conditionally stable.

The analysis of each of the systems with up to four high-pass filters can be carried out in a similar manner to that discussed above and the results are shown in Table 1 for the approximations of $\zeta \ll 1$ and $\alpha \gg 1$. It is evident from Table 1 that the maximum non-dimensional gain for the acceleration feedback control system is smaller than the corresponding maximum non-dimensional gains for velocity feedback because it is a function of the system-damping ratio. Thus velocity and displacement feedback control potentially have much larger stability limits.

The closed-loop responses for the realistic systems can be calculated by substituting for $G(\mathrm{j}\Omega)$ from Eq. (2) together with the appropriate $H(\mathrm{j}\Omega)$, into Eq. (1). The closed-loop mobilities for acceleration, velocity and displacement feedback control systems with one, two and three high-pass filters respectively are plotted in Fig. 4 with 99.9% of the respective maximum gains with high-pass filters present, to make the effects clear. The closed-loop mobilities for zero gain and for the ideal systems are also plotted for comparison. The frequencies at which the systems become unstable are evident by narrow peaks and are tabulated in Table 2. It is clear from Fig. 4 that acceleration feedback control is not a realistic practical option as it has limited effect before it becomes unstable with a single high-pass filter. Displacement feedback introduces a second resonance peak at the critical frequency. It seems that velocity feedback control is, however, a robust and realistic control strategy.

Table 1
Non-dimensional maximum gains for different numbers of high-pass filters, $\alpha \gg 1$ and $\zeta \ll 1$

Number of high-pass filters	Acceleration feedback	Velocity feedback	Displacement feedback
0	Unconditionally stable	Unconditionally stable	Unconditionally stable
1	$\frac{g_{\max}}{m} \approx 2\zeta\,\alpha$	Unconditionally stable	Unconditionally stable
2	$\frac{g_{\max}}{m} \approx \zeta\,\alpha$	$\frac{g_{\max}}{c_{\mathrm{crit}}} \approx \alpha$	Unconditionally stable
3	—	$\frac{g_{\max}}{c_{\mathrm{crit}}} \approx \frac{4}{9}\alpha$	$\frac{g_{\max}}{k} \approx 8$
4	—	—	$\frac{g_{\max}}{k} \approx 4$

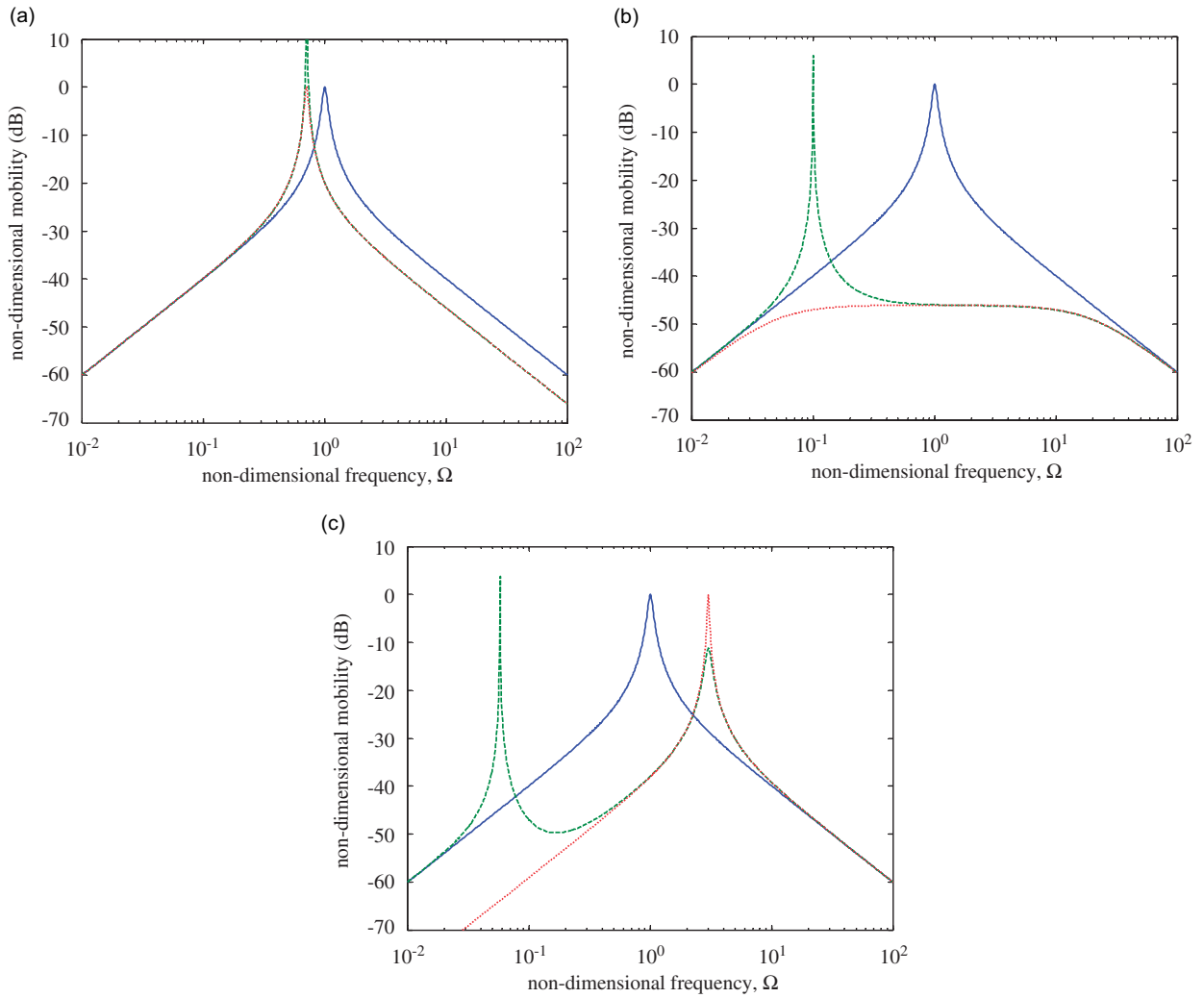

Fig. 4. Closed-loop response of a single-degree-of-freedom system, $\zeta = 0.05$; no control, solid line; ideal system with gains of 99.9% of maximum with the high-pass filters present, dotted line; realistic system with high pass filters and gains of 99.9% of maximum, dashed line. (a) Acceleration feedback $g_{\max}/m = \alpha\zeta$ with one high-pass filters, (b) velocity feedback $g_{\max}/c_{\text{crit}} = 4\alpha/9$ with two high-pass filters and (c) displacement feedback $g_{\max}/k = 4$ with three high-pass filters.

4. Instability due to phase-lag (time delay)

In a real system, phase-lag in the control system will be present due to the dynamics of transducers such as the accelerometers or secondary force shaker, and any low-pass filters used. Time delay will also occur in digital control systems. For simplicity, the instabilities that occur due to the high frequency dynamics are considered by assuming a pure time delay in the feedback loop. It is represented in the frequency domain as $e^{-j2\pi\tau\Omega}$, where $\tau = T/T_n$ is the normalised delay, T_n is the natural period of the plant and T is the physical time delay. The method of analysis to determine the critical frequency at which the system becomes unstable, and the maximum gain that can be applied before the system becomes unstable, is similar to that described in Section 3.

First consider time delay introduced into a system with acceleration feedback control. The open-loop response is given by

$$G(j\Omega)H(j\Omega) = \left(\frac{g}{m}\right)\left(\frac{-\Omega^2}{1-\Omega^2+j2\zeta\Omega}\right)e^{-j2\pi\,\Omega\tau}. \tag{11}$$

Table 2
Non-dimensional frequencies at which the feedback systems become unstable, $\alpha \gg 1$ and $\zeta \ll 1$

Number of high-pass filters	Acceleration feedback	Velocity feedback	Displacement feedback
0	Unconditionally stable	Unconditionally stable	Unconditionally stable
1	$\Omega_c \approx \frac{1}{\sqrt{1+2\zeta\alpha}}$	Unconditionally stable	Unconditionally stable
2	$\Omega_c \approx \frac{1}{\sqrt{1+\zeta\alpha}}$	$\Omega_c \approx \frac{1}{\alpha}$	Unconditionally stable
3	—	$\Omega_c \approx \frac{\sqrt{3}}{\alpha}$	$\Omega_c \approx \frac{1}{\sqrt{3}\alpha}$
4	—	—	$\Omega_c \approx \frac{1}{\alpha}$

Following the procedure in Section 3, the imaginary part of Eq. (11) is set to zero and solved to give the frequency at which the system becomes unstable. This results in $\tan(2\pi\tau\Omega_c) = -2\zeta\Omega_c/(1-\Omega_c^2)$. For low damping, when $\zeta \ll 1$, and for $\tau \ll 1$ the critical frequency is given by

$$\Omega_c \approx \frac{1}{2\tau}. \tag{12}$$

Substituting the approximate critical frequency given in Eq. (12) into the real part of Eq. (11) and equating to -1, gives the maximum non-dimensional gain, before the system becomes unstable. Assuming $4\tau^2 < 1$, this gives

$$\frac{g_{\max}}{m} \approx 1. \tag{13}$$

Next, consider time delay introduced into a system with velocity feedback control. The open-loop response is given by

$$G(\mathrm{j}\Omega)H(\mathrm{j}\Omega) = \left(\frac{g}{c}\right)\left(\frac{\mathrm{j}2\zeta\Omega}{1-\Omega^2+\mathrm{j}2\zeta\Omega}\right)\mathrm{e}^{-\mathrm{j}2\pi\Omega\tau}. \tag{14}$$

Setting the imaginary part of Eq. (14) to zero yields $\tan(2\pi\tau\Omega_c) = (1-\Omega_c^2)/(2\zeta\Omega_c)$. When $\zeta \ll 1$ and $\tau \ll 1$ the critical frequency is thus given by

$$\Omega_c \approx \frac{1}{4\tau} \tag{15}$$

and the resulting maximum gain is given by $g_{\max}/c \approx (1-16\tau^2)/8\tau$. If $16\tau^2 \ll 1$ this reduces to the very simple criterion for the maximum gain of

$$\frac{g_{\max}}{c_{\mathrm{crit}}} \approx \frac{1}{8\tau}. \tag{16}$$

Finally, consider time delay introduced into a system with displacement feedback control. The open-loop response is given by

$$G(\mathrm{j}\Omega)H(\mathrm{j}\Omega) = \left(\frac{g}{k}\right)\left(\frac{1}{1-\Omega^2+\mathrm{j}2\zeta\Omega}\right)\mathrm{e}^{-\mathrm{j}2\pi\Omega\tau}, \tag{17}$$

which following the procedure above yields $\tan(2\pi\tau\Omega_c) = -2\zeta\Omega_c/(1-\Omega_c^2)$. When $\zeta \ll 1$ and $\tau \ll 1$ the critical frequency is thus given by

$$\Omega_c \approx 1 + \frac{\zeta}{2\pi\tau} \tag{18}$$

and the resulting maximum gain is given by

$$\frac{g_{\max}}{k} \approx \frac{\zeta}{\pi\tau}. \tag{19}$$

Table 3
Non-dimensional frequencies at which the feedback systems become unstable and the maximum gains that can be applied for a non-dimensional time-delay τ, in the control system. $\tau \ll 1$ and $\zeta \ll 1$

	Acceleration feedback	Velocity feedback	Displacement feedback
Critical frequency	$\Omega_c \approx \frac{1}{2\tau}$	$\Omega_c \approx \frac{1}{4\tau}$	$\Omega_c \approx 1 + \frac{\zeta}{2\pi\tau}$
Non-dimensional maximum gain	$\frac{g_{\max}}{m} \approx 1$	$\frac{g_{\max}}{c_{\text{crit}}} \approx \frac{1}{8\tau}$	$\frac{g_{\max}}{k} \approx \frac{\zeta}{\pi\tau}$

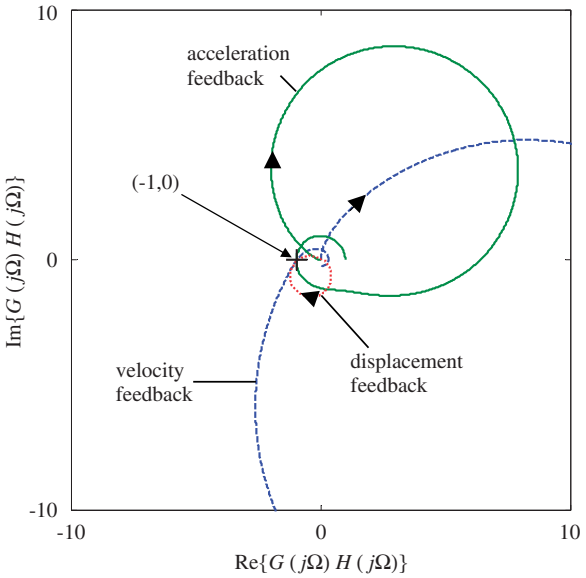

Fig. 5. Nyquist open-loop response plots for a non-dimensional time delay of 0.1, $\zeta = 0.05$. The maximum feedback gain has been used in each system so that all the plots pass through the point $(-1, 0)$. Acceleration feedback, solid line; velocity feedback, dashed line; displacement feedback, dotted line.

The critical frequencies and corresponding maximum gains for the systems with time delay are given in Table 3. The Nyquist plots for the three control strategies each with a non-dimensional time delay of 0.1 are plotted for 99.9% of the respective maximum gains in Fig. 5. It can be seen that all the curves cross the negative real axis as expected. The overall magnitude of the Nyquist plot is, however, much larger for velocity feedback than it is for either displacement or acceleration feedback. The closed-loop responses for the systems with 99.9% of the respective maximum gains are plotted in Fig. 6 together with the ideal systems having similar gains. It can be seen that there are many additional resonance frequencies in the system with acceleration feedback control, making this control system impractical for reasonably large time delays in the control system.

5. Experimental work

To validate the theoretical predictions, experimental work was carried out on a sdof system set on a rigid foundation as shown in Fig. 7a. It consisted of a 2.9 kg aluminium plate (that behaved as a rigid-body at frequencies up to 1 kHz) and two passive mounts that were placed symmetrically beneath the plate, each of which had a stiffness of 2.4 kN m^{-1} and damping coefficient of 18 Ns m^{-1}. Two electromagnetic shakers driven by the same control voltage produce the active force, which was transmitted to the bottom discs by thin rods

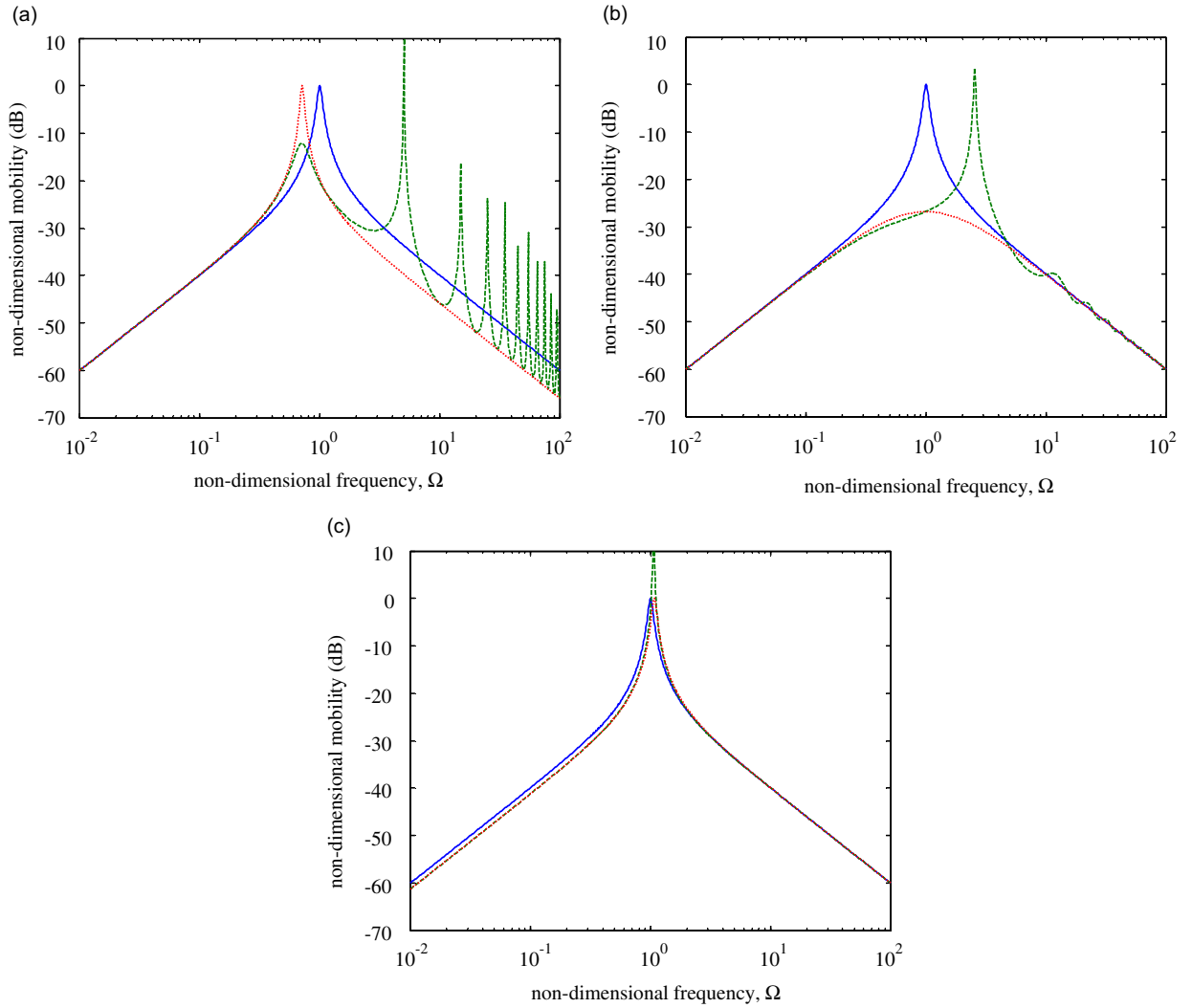

Fig. 6. Closed-loop response—effects of time delay, $\tau = 0.1$, $\zeta = 0.05$ no control, solid line; system with time delay and 99.9% of maximum gain, dashed line; ideal system, dotted line: (a) acceleration feedback control, (b) velocity feedback control and (c) displacement feedback control.

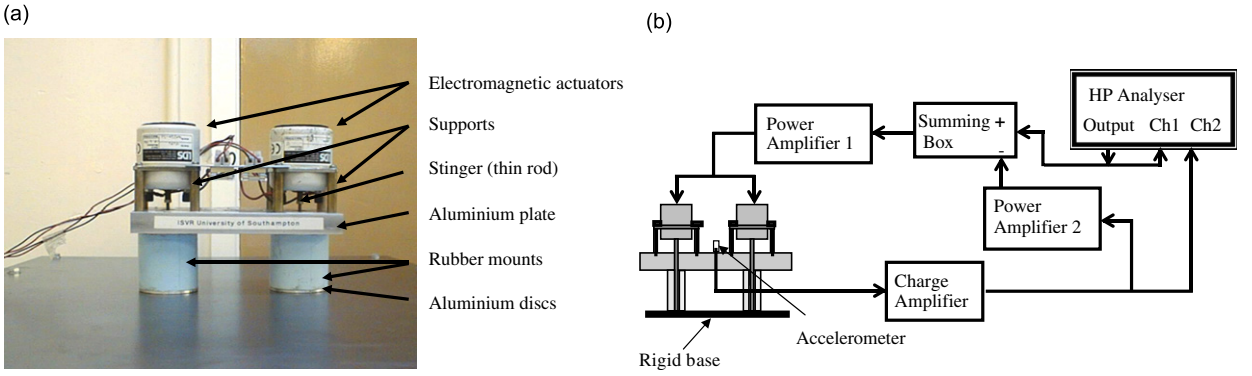

Fig. 7. Experimental set-up for feedback control of the single-degree-of-freedom system: (a) two-mount active control system and (b) experimental control system.

through the rubber cylinders. Since it was a symmetric system with respect to the mass centre of the aluminium plate, it was possible to treat the system as a sdof system. The experimental set-up is shown in Fig. 7b.

The frequency responses of the power amplifiers and the charge amplifiers were measured and first-order models were fitted to these data. These models were then incorporated into the open- and closed-loop feedback model and the response of the system calculated. The simulated and measured Nyquist plots are shown in Figs. 8a–d for acceleration, velocity and displacement feedback with various high-pass filter corner frequencies. It can be seen in Fig. 8a that the Nyquist plot for acceleration feedback crosses the negative real axis for very small gain. In Figs. 8b and c, it can be seen that for velocity feedback the maximum gain that can be applied is reduced as the cut-off frequency of the charge amplifier is increased. This is in qualitative agreement with the predictions given in Table 1. In Fig. 8d it can be seen that with displacement feedback control there is better low frequency stability.

In Fig. 9 the theoretical and experimental closed-loop responses for the system with velocity feedback are plotted for charge amplifier cut-off frequencies of 1 and 10 Hz. The maximum gain applied in these plots is the

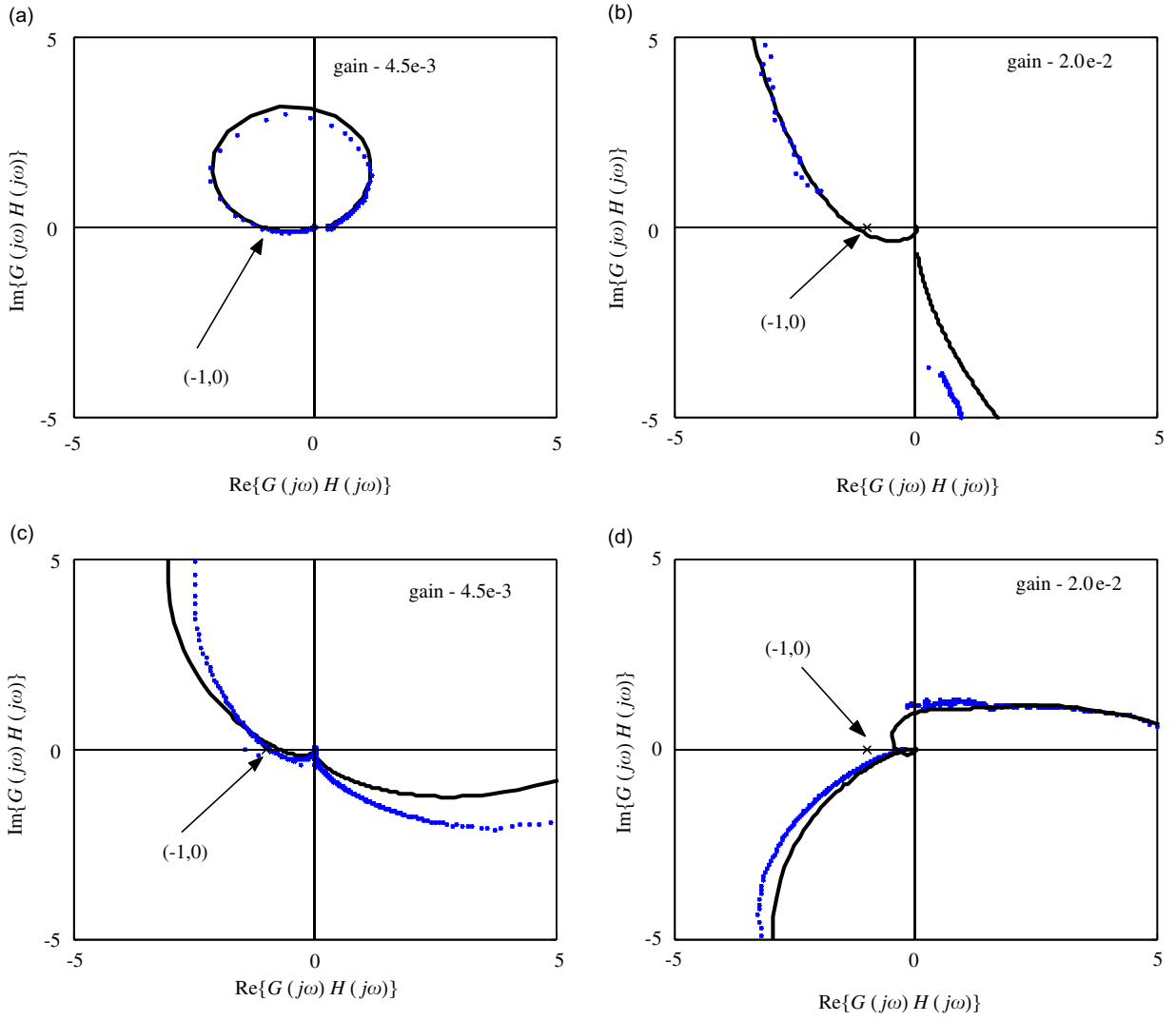

Fig. 8. Nyquist plots for acceleration, velocity and displacement feedback control. Simulation, solid line; experiment, dotted line: (a) acceleration feedback 0.2 Hz cut-off, (b) velocity feedback 1 Hz cut-off, (c) velocity feedback 10 Hz cut-off and (d) displacement feedback 1 Hz cut-off.

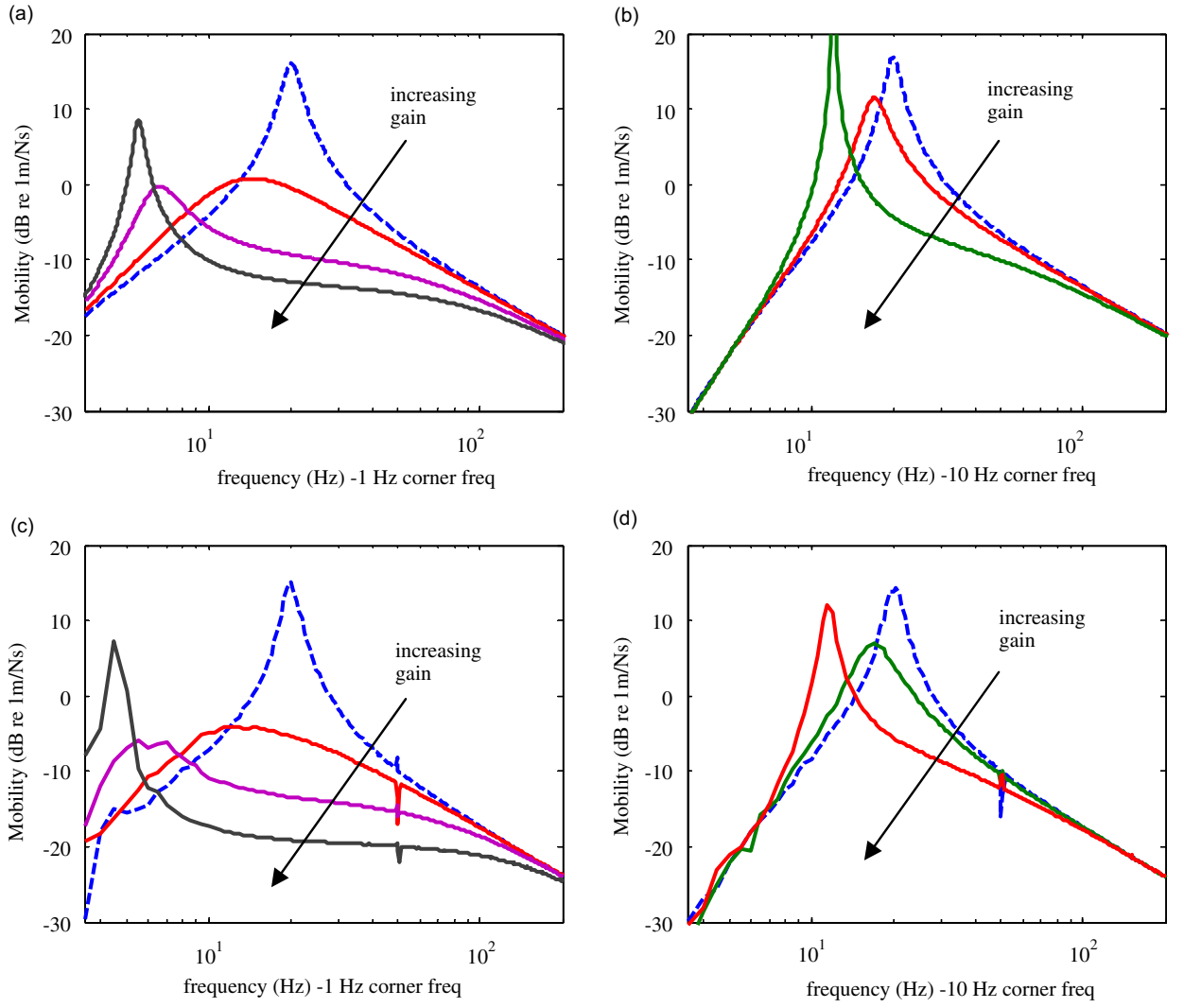

Fig. 9. Closed-loop frequency responses for velocity feedback control. Charge amplifier cut-off frequency set to 1 Hz or 10 Hz; no control, dashed line; with control, solid line: (a) simulation 1 Hz cut-off, (b) simulation 10 Hz cut-off, (c) measurement 1 Hz cut-off and (d) measurement 10 Hz cut-off.

gain just before the system becomes unstable. It is clear from this figure that the cut-off frequency of the charge amplifier has a profound effect on the maximum gain and hence the performance, as discussed in Section 3.

6. Discussion

The important results in this paper are given in Tables 1–3, and enable some qualitative statements to be made about the control systems. As noted above, velocity feedback control is the most attractive strategy for active vibration isolation as it is robust to both low frequency phase-lead and time delays in the control loop (phase-lag). Inspection of Tables 1 and 3, shows that it is desirable for the natural frequency of the system to be much higher than the corner frequency of the high-pass filters. These are key points in the design of an active vibration isolation system and were incorporated in the prototype system reported in Ref. [14], resulting in very good performance.

Tables 1 and 3 also show that if acceleration feedback control is very sensitive to the phase-lead due to the instrumentation at low frequencies, and displacement feedback is very sensitive to time delays in the feedback loop. In both these cases, high damping in the isolator is desirable.

7. Conclusions

This paper has described an investigation into stability issues of an active vibration control system due to the hardware in the control system. To this end, a sdof system has been studied, with acceleration, velocity and displacement feedback control applied. Two regimes have been identified; a low frequency regime where the instability is caused by the phase advance in the high-pass filters, and a high frequency regime where the instability is caused by time delay, or phase-lag. Simple formulae have been derived which give the frequency at which the system becomes unstable, and the maximum gain that can be applied to each system. These formulae give insight into how the physical parameters govern the instabilities. It has been shown that for acceleration and velocity feedback control it is desirable to have a high plant natural frequency compared to the corner frequency of the high-pass filter. However, it is desirable to have high damping of displacement and acceleration feedback. Some experimental work is has also been presented to support the theoretical results.

References

[1] R.C. Dorf, *Modern Control Systems*, Addison Wesley-Publishing Company, Reading, MA, 1967.
[2] M.J. Balas, Direct velocity feedback control of large space structures, *Journal of Guidance and Control* 2 (1979) 252–253.
[3] M. Serrand, S.J. Elliott, Multichannel feedback control for the isolation of base-excited vibration, *Journal of Sound and Vibration* 234 (2000) 681–704.
[4] S.J. Elliott, M. Serrand, P. Gardonio, Feedback stability limits for active isolation systems with reactive and inertial actuators, *Transactions of the ASME, Journal of Vibration and Acoustics* 123 (2001) 250–261.
[5] S.M. Kim, S.J. Elliott, M.J. Brennan, Decentralised control for multichannel active vibration isolation, *IEEE Transactions on Control Systems Technology* 9 (1) (2001) 93–100.
[6] T. Hodges, The Active Simulation and Modification of Structural Frequency Response, PhD Thesis, University of Southampton, UK, 1989.
[7] C.R. Fuller, S.J. Elliott, P.A. Nelson, *Active Control of Vibration*, Academic Press Ltd, London, 1996.
[8] A. Preumont, *Vibration Control of Active Structures: An Introduction*, Kluwer Academic Publishers, Dordrecht, 2002.
[9] M.Z. Ren, K. Seto, F. Doi, Feedback structure-borne sound control of a flexible plate with an electromagnetic actuator: The phase lag problem, *Journal of Sound and Vibration* 205 (1) (1997) 57–80.
[10] A.K. Agrawal, J.N. Yang, Effect of fixed time delay on stability and performance of actively controlled civil engineering structures, *Earthquake Engineering and Structural Dynamics* 26 (1997) 1169–1185.
[11] C.J. Goh, T.K. Caughey, On the stability problem caused by finite actuator dynamics in the collocated control of large space structures, *International Journal of Control* 41 (3) (1985) 787–802.
[12] J.L. Fanson, T.K. Caughey, Positive position feedback control for large space structures, *AIAA Journal* 28 (4) (1990).
[13] M.I. Friswell, D.J. Inman, The relationship between positive position feedback and output feedback controllers, *Smart Materials and Structures* 8 (1999) 285–291.
[14] M.J. Brennan, S.J. Elliott, X. Huang, A demonstration of active vibration isolation using decentralised velocity feedback control, *Smart Materials and Structures* 14 (206) (2004) N1–N4.